Molecules and Cells

Insight into Structural Aspects of Histidine 284 of *Daphnia magna* Arginine Kinase

Zhili Rao[1,4], So Young Kim[1,4], Xiaotong Li[1], Da Som Kim[1], Yong Ju Kim[2,3,*], and Jung Hee Park[1,3,*]

[1]Division of Biotechnology, College of Environmental & Bioresources Sciences, Jeonbuk National University, Iksan 54596, Korea, [2]Department of Herbal Medicine Resources, College of Environmental and Bioresource Sciences, Jeonbuk National University, Iksan 54596, Korea, [3]Advanced Institute of Environment and Bioscience, College of Environmental & Bioresources Sciences, Jeonbuk National University, Iksan 54596, Korea, [4]These authors contributed equally to this work.
*Correspondence: nationface@jbnu.ac.kr (YJK); junghee.park@jbnu.ac.kr (JHP)
https://doi.org/10.14348/molcells.2020.0136
www.molcells.org

Arginine kinase (AK), a bioenergy-related enzyme, is distributed widely in invertebrates. The role of highly conserved histidines in AKs is still unascertained. In this study, the highly conserved histidine 284 (H284) in AK of *Daphnia magna* (*Dm*AK) was replaced with alanine to elucidate the role of H284. We examined the alteration of catalytic activity and structural changes of H284A in *Dm*AK. The catalytic activity of H284A was reduced dramatically compared to that in wild type (WT). Thus the crystal structure of H284A displayed several structural changes, including the alteration of D324, a hydrogen-bonding network around H284, and the disruption of π-stacking between the imidazole group of the H284 residue and the adenine ring of ATP. These findings suggest that such alterations might affect a conformational change of the specific loop consisting of G310-V322 at the antiparallel β-sheet region. Thus, we speculated that the H284 residue might play an important role in the conformational change of the specific loop when ATP binds to the substrate-binding site of *Dm*AK.

Keywords: arginine kinase, crystallization, kinetics, point mutation, X-ray crystallography

INTRODUCTION

Phosphagen kinases (PKs) are a family of phosphotransferases that reversibly catalyze the delivery of high-energy phosphoryl groups between ATP and guanidine derivatives. The phosphorylated guanidines, also known as phosphagens, are a type of high-energy compounds that play an important role in cellular energy homeostasis in both the muscles and the brain by providing a way to store high-energy phosphates as a metastable compound (Ellington, 2001). PKs are widespread in all types of animal cells that require considerable amounts of energy. Eight PKs have been reported in invertebrates (Ellington, 1989; Uda et al., 2005). One of these, arginine kinase (AK), is distributed widely in invertebrates, and its activity has also been observed in arthropods, mollusks, nematodes, protozoans, and some bacteria (Ellington, 1989; Newsholme et al., 1978).

Arginine, which is an essential amino acid in many organisms, is produced as an intermediate in two regulatory cycles: the urea and the nitric oxide cycles (Noh et al., 2002). This intermediate is also used by AK to maintain energy homeostasis in cells. AK requires both arginine and ATP as bi-substrates and plays a key role in catalyzing the reversible transfer of the γ-phosphoryl group of ATP to the guanidine functional group of arginine (Adeyemi and Whiteley, 2014; Alonso et al., 2001; Hansen and Knowles, 1981; Wyss and

Received 19 June, 2020; revised 29 July, 2020; accepted 10 August, 2020; published online 31 August, 2020

eISSN: 0219-1032

Kaddurah-Daouk, 2000; Zhou et al., 1998). In particular, AK activity is required for muscle contraction and the generation of electrical conductance in nerves. Many functional and structural studies of AKs from diverse organisms have been reported in a substrate-binding-dependent manner (Azzi et al., 2004; Brown and Grossman, 2004; Fernandez et al., 2007; Niu et al., 2011; Pruett et al., 2003; Watts et al., 1980). The overall topology of AKs commonly has two different domains: an N-terminal domain, which consists of small α-helices, and a C-terminal domain, which comprises an eight-strand antiparallel β-sheet connected by α-helices. In AKs, the N-terminal domain can interact with arginine (i.e., either L-arginine or phosphoarginine), whereas the central role of the C-terminal domain is nucleotide-binding (i.e., either ATP or ADP) (Fernandez et al., 2007; Zhou et al., 1998). In the structural comparison between *Trypanosoma cruzi* AK_{apo} (*Tc*AK_{apo}) and *Limulus Polyphemus* AK_{holo} (*Lp*AK_{holo}), some structural changes accompanied by rigid-body motion of the helix and the antiparallel β-sheet outward from the nucleotide-binding site in the C-terminal domain were observed significantly (Clark et al., 2012; Fernandez et al., 2007). In addition, the structural changes in the substrate-bound (holo) and the substrate-free (apo) state of AK have been confirmed by joint crystallographic and NMR residual dipolar coupling analysis (Niu et al., 2011). Thus, the results indicated that the two different AK conformations might derive from substrate-induced motion.

Several highly conserved residues in the arginine and ATP binding sites that alter AK enzyme activity have been reported (Guo et al., 2004; Strong and Ellington, 1996; Takeuchi et al., 2004; Wu et al., 2014). In *Nautilus* and *Stichophus* AKs, the mutations of D62G and R193G accompanying the disappearance of the salt bridge showed considerably decreased activity. Hence, the mutagenesis of both D62G and R193G has been proposed to be associated with structural stability and bi-substrates' affinity (Suzuki et al., 2000a; 2000b). On the other hand, the mutations of C271, P272 and T273 replaced with alanine, which are located at the hinge loop in AKs, showed reduced activity in the previous studies (Liu et al., 2011; Strong and Ellington, 1996; Wu et al., 2008; 2014). These findings revealed an alteration of enzyme activity due to structural changes at the arginine binding site. Thus, these residues were confirmed as key players in the substrate synergism between the arginine residues (L-arginine and phosphoarginine) of AK and their constraining position (Wu et al., 2014). In the transition state analog (TSA) including nitrate (NO_3), the crystal structure of AK from horseshoe crab revealed the relationship between nitrate and the bi-substrate (Zhou et al., 1998). The substrate arginine showed two salt bridges with E225 and E314. Hence, the variants of E225 and E314 exhibited alteration of catalytic activity with a reduced rate of production of phosphoarginine and ADP (Pruett et al., 2003).

Although several mutagenesis studies have reported highly conserved residues at the arginine binding site of AKs, a role has not yet been elucidated for the highly conserved histidine residue H284 around the ATP binding site. This study is the first report of the crystal structure of wild-type *Dm*AK (*Dm*AK WT) and its H284A mutant. Based on the introduction of H284A to *Dm*AK, some structural alterations of the surrounding residue were detected, i.e., the disruption of π-stacking between the imidazole group of the H284 residue and the adenine ring of ATP, the alteration of D324, and a hydrogen-bonding network around H284. These findings may be important clues for explaining the effects of H284A on the reduction of activity compared with WT. Therefore, our results provide a clue to improve our understanding of the bioenergetics mechanism.

MATERIALS AND METHODS

Cloning, expression, and purification of *Dm*AK WT and H284A

The *Dm*AK gene was synthesized according to the full-length open reading frame (GenBank accession No. AID69955.1) from National Center for Biotechnology Information (NCBI; http://www.ncbi.nlm.nih.gov). The synthesized gene was amplified by a standard PCR method with a primer set (5′-GCACTCCATATGCATCACCATCATCATCATGTGGAC-3′ and 5′-GCACTCGCGG CCGCTTATGCGGC TTC-3′) and inserted into an expression vector (pET30a; New England Biolabs, USA) using *Nde*I and *Not*I restriction enzyme sites. A six-His tag was fused to the N-terminus of the gene to facilitate protein purification. The mutation was introduced by modified overlap PCR using a single site mismatched primer against H284 (5′-GCAGTGCAATGGCCACTGAGGCCC-3′). The recombinant construct was transformed into *Escherichia coli* BL21 (DE3) cells. Then, overnight cultures of the transformed cells were transferred to 1 L of LB broth (BD Bioscience, USA) containing kanamycin (Duchefa Biochemie, The Netherlands), with a final concentration of 50 μg/ml, and incubated at 37°C and 200 rpm until reaching the optical density of 0.6 at 600 nm (OD_{600}). Large quantities of recombinant *Dm*AK proteins were obtained by inducing the expression of *Dm*AK WT and H284A with 0.5 mM isopropyl β-D-1-thiogalactopyranoside (IPTG) (Duchefa Biochemie) for 4 h at 18°C and 170 rpm. The harvested cells were resuspended in 20 ml of buffer (10 mM Tris-HCl, pH 8.0, 100 mM NaCl) and lysed for 2 min by sonication (4 s sonication and 4 s rest) (Sonics and Materials, USA). The cellular debris was removed by centrifugation (12,000 rpm, 4°C) for 20 min, and then the supernatant was purified using affinity chromatography with a HisTrap FF column (GE Healthcare, USA) (Rao et al., 2019). To ensure the high purity of *Dm*AK WT and H284A, the HiTrap Q FF column (GE Healthcare) was used with a double gradient elution buffer system (10 mM Tris-HCl, pH 7.0, 1 M NaCl). The purified *Dm*AK was analyzed by 12% SDS-PAGE (Supplementary Method), and Bradford's method was employed to ascertain the protein concentration (Bradford, 1976).

Enzyme assay and determination of kinetic parameters

To ascertain the optimal pH and temperature, AK activity was conducted as described previously (Li et al., 2006; Pereira et al., 2000; Wu et al., 2014). For the optimal pH and temperature determination, enzyme activity was measured in 100 mM sodium citrate-citrate buffers at pH 5.5-6.5, 100 mM Tris-HCl buffers at pH 7.0-9.0, and 100 mM glycine-NaOH buffers at pH 9.5-10.0 in the temperature range from the

0°C to 70°C, respectively. The reaction mixture for the AK assay contained freshly prepared 10 mM L-arginine, 2 mM ATP, and 3 mM magnesium acetate in 100 mM Tris-HCl, pH 8.5. To initiate the enzyme reaction, we added 30 μl of *Dm*AK WT and H284A (*Dm*AKs) solutions at different concentrations to the 270 μl of the reaction mixture. After 1 min, we halted the reaction by adding 2.5% trichloroacetic acid (TCA). The reaction mixture was heated for 1 min at 100°C and then cooled immediately in ice-water for 1 min. The cooled samples were incubated at room temperature for 5 min, and the inorganic phosphate level was ascertained using a phosphate determination reagent (Baoyu et al., 2003). We measured the absorbance at 660 nm at room temperature using a UV-Vis spectrophotometer (Infinite 200® Pro; Tecan, Austria). All measurements were conducted more than three times with once-purified *Dm*AKs.

Crystallization and structure determination of *Dm*AK WT and H284A

Purified *Dm*AKs were concentrated using a Centricon concentrator (10 kDa molecular weight cut-off membrane; Millipore, USA). The Bradford assay has been used to check over 10 mg/ml of *Dm*AKs (Bradford, 1976). The initial crystallization trials were performed using commercial screening kits: a Quik screen, a Grid screen of Ammonium Sulfate, and a PEG-ion kit (Hampton research). In the hanging drop vapor diffusion method, protein droplets of 3 μl were mixed with a reservoir solution of 3 μl in a 24-well VDX plate (Hampton research). The plate was incubated at 20°C, and single crystals of *Dm*AKs appeared in the crystallization buffer (1.8 M potassium phosphate, pH 8.2) within three days.

Data collection for the *Dm*AK crystals was achieved by freezing single crystals gradually in liquid nitrogen using 5% to 10% sucrose under crystallization conditions. We collected the diffraction data for *Dm*AK crystals using an ADSC Quantum 270 CCD detector on beamline 7A at Pohang Accelerator Laboratory (Korea). All data were indexed, integrated, and scaled using the XDS software package (Kabsch, 2010). Two different structures were solved by molecular replacement using the PHASER program with an AK template (PDB ID code 4BHL; sequence identity 78.3%) (Lopez-Zavala et al., 2013; McCoy et al., 2007). Each DmAK model was rebuilt

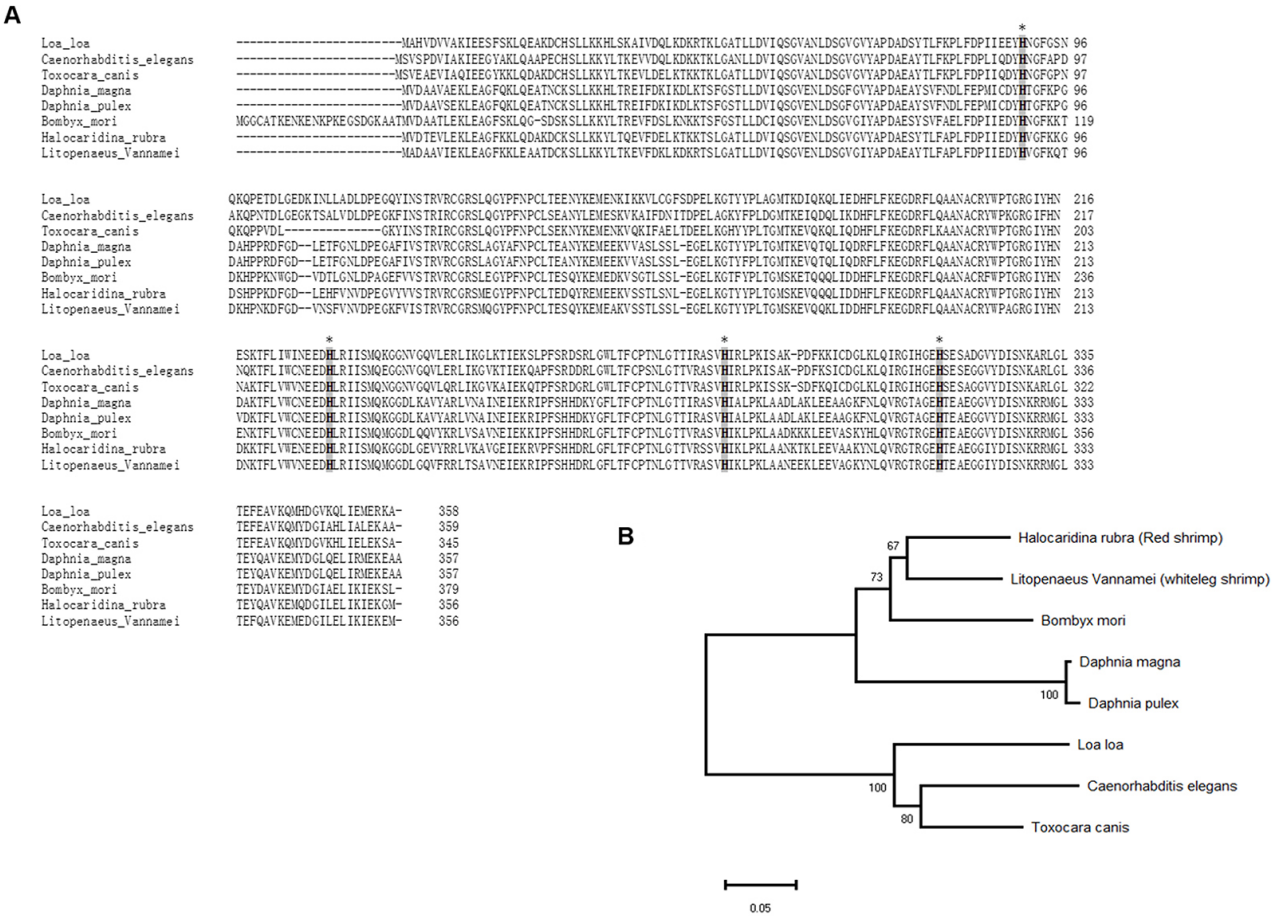

Fig. 1. Multiple sequence alignment and phylogenetic analysis of AKs. (A) Alignment of *Dm*AK and other AKs from arthropods and nematodes. Highly conserved histidine residues are labeled with gray color and asterisks. (B) The phylogenetic tree of AKs in various organisms. The Neighbor-Joining method was used for inferring the evolutionary history, and the branch length and bootstrap values were obtained from 1,000 replicates.

and refined at 1.87 Å of *Dm*AK WT in the apo state (*Dm*AK WT_{apo}) and 1.34 Å of L-arginine-binding H284A (*Dm*AK H284A-Arg), respectively. Further building and refining of the models were performed using the Coot and Refmac5 program (Emsley and Cowtan, 2004; Murshudov et al., 1997). After the final refinement, the models were validated using the Worldwide Protein Data Bank server (wwPDB; https://validate-rcsb-2.wwpdb.org/) to deposit the structures of *Dm*AKs. The coordinate and structural factor of *Dm*AK WT_{apo} and *Dm*AK H284A-Arg were deposited in the wwPDB with the accession codes 6KY2 and 6KY3, respectively. The crystallographic data collection and refinement statistics are provided in Supplementary Table S1. All figures were provided by PyMol (Schrödinger, 2010).

RESULTS AND DISCUSSION

Multiple sequence alignment of the *Dm*AK gene with other AKs

The *Dm*AK gene was annotated as an AK in the freshwater flea *D. magna*. The *Dm*AK amino acid sequence was aligned with those of several AKs from arthropods and nematodes using the Clustal Omega tool from EBI (www.ebi.ac.uk) (Fig. 1A). In most of the AKs, some amino acids were highly conserved in the substrate-binding region, whereas the amino acid sequences of each AK were different at the N-terminus. The sequence identity of *Dm*AK showed 98.88% similarity with AK from the *Daphnia* genus, but the sequence identities of AKs from other phyla were less than 80% similarity. We constructed the phylogenetic tree using the neighbor-joining method in the MEGA X program (Fig. 1B): it shows two clusters, according to the phylum. One cluster contains *Halocaridina rubra*, *Litopenaeus vannamei*, *Bombyx mori*, *Daphnia pulex*, and *Daphnia magna*, and the other cluster contains *Loa loa*, *Toxocara canis*, and *Caenorhabditis elegans*. The phenogram indicates that *Dm*AK is closer to the arthropod phyla than to the nematode phyla.

To date, the roles of highly conserved amino acids, i.e., D62, R193, E225, C271, P272, T273, and E314, in AKs have been elucidated using mutagenesis in previously biochemical and biophysical studies (Guo et al., 2004; Liu et al., 2011; Pruett et al., 2003; Strong and Ellington, 1996; Suzuki et al., 2000a; 2000b; Wu et al., 2008; 2014). Furthermore, five histidine residues are well conserved in PKs. The role of each histidine of creatine kinase (CK) in vertebrates has been reported in biochemical and biophysical studies (Chen et al., 1996; Forstner et al., 1997; Muhlebach et al., 1994). Specifically, histidine residues (H96, H105, H190, H233, and H295) from rabbit muscle CK were studied using site-directed mutagenesis, which was replaced with asparagine (Chen et al., 1996). According to the results, H295N located at the active site of rabbit CK showed dramatically reduced enzyme activity compared with the native form; however, the exact roles of H295 still remains a question (Chen et al., 1996). In this study, we focused on H284 of *Dm*AK replaced with alanine (H284A), corresponding to H295 in rabbit CK, highly conserved in several invertebrates as shown in Fig. 1A.

Enzyme kinetics of *Dm*AK WT and H284A

The overexpressed *Dm*AK WT and H284A proteins containing the 6-histidine tag at the N-terminus were purified by affinity and ion-exchange chromatography. Purified *Dm*AK WT and H284A were detected with an estimated molecular weight of approximately 41 kDa (Supplementary Fig. S1). The final yield of *Dm*AKs was 5 mg/L, and the purity was approximately 99%. The purified proteins were used to measure enzyme kinetics and crystallization.

Steady-state kinetic measurements of *Dm*AK WT and H284A mutant were made at optimum pH and temperature (Supplementary Fig. S2), using the forward reaction. In contrast to *Dm*AK WT, the activity of H284A was dramatically reduced in enzyme concentration ranged from 0 to 3.2 μM (final concentration). The relative activity of H284A was approximately four times lower than that of *Dm*AK WT at the highest enzyme concentration (Fig. 2). The values of V_{max} and k_{cat} of H284A were also decreased dramatically, compared with those of *Dm*AK WT. Table 1 shows the kinetic parameters, including V_{max}, k_{cat}, and K_d, for L-arginine and ATP. According to our results, H284A showed an approximately 10-fold lower V_{max} value and a 100-fold decreased turnover number (k_{cat}) than *Dm*AK WT. Despite the reduction in catalytic efficiency, the K_m values of H284A for both substrates were similar to that of *Dm*AK WT. The average K_m^{Arg} and K_m^{ATP} values of *Dm*AK WT/H284A were 0.90/0.90 mM and

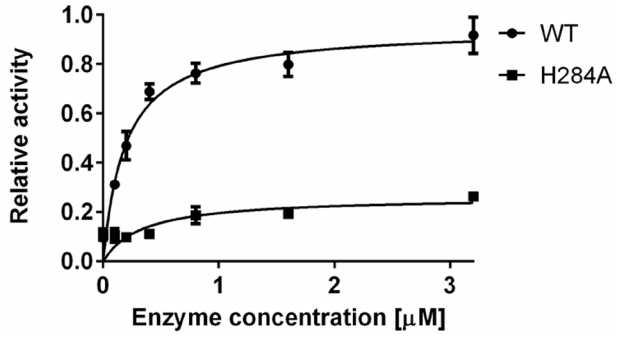

Fig. 2. Kinetic analysis of *Dm*AK WT and H284A in an enzyme concentration-dependent manner. Enzyme concentrations in the system ranged from 0 to 3.2 μM, and the relative initial rates were plotted.

Table 1. Comparison of the forward reaction parameters of *Dm*AK WT and H284A

	V_{max} (μmolpimin^{-1}mg^{-1})	K_{cat} (s^{-1})	K_m^{Arg} (mM)	K_d^{Arg} (mM)	K_m^{ATP} (mM)	K_d^{ATP} (mM)
*Dm*AK WT	111.6 ± 3.61	18.6 ± 0.60	0.90 ± 0.11	0.74 ± 0.10	0.47 ± 0.07	0.87 ± 0.12
*Dm*AK H284A	11.66 ± 1.23	0.19 ± 0.02	0.90 ± 0.45	0.41 ± 0.21	0.30 ± 0.12	1.01 ± 0.44

0.47/0.30 mM for arginine (K_m^{Arg}) and ATP (K_m^{ATP}), respectively (Table 1). The catalytic turnover rate of H284A was only 1.02% of that of *Dm*AK WT, and the k_{cat}/K_m values for L-arginine and ATP of H284A were reduced to 1% and 1.6% of those of *Dm*AK WT, respectively. These findings are consistent with the previously reported k_{cat} values of C271 mutants from horseshoe crab AK (Gattis et al., 2004). This finding suggests that the reduced enzyme activity was not due to inhibition of their substrate binding.

Moreover, the dissociation constant (K_d^{Arg}) value for L-arginine was 0.41 ± 0.21 mM, which is slightly less than that of *Dm*AK WT, whereas the dissociation constant (K_d^{ATP}) value for ATP was 1.01 ± 0.44 mM, which is larger than that of *Dm*AK WT (Table 1). However, the values did not show any significant difference. Although the activity of H284A was dramatically decreased, it was not enough to explain the role of H284 (Fig. 2). Thereby the structural analysis of H284A was necessary to investigate the cause of reduction of H284A activity at the molecular level to more accurately.

Overall structures of *Dm*AK WT in the apo-state and its mutant with arginine

The crystallized *Dm*AK WT_{apo} in the apo-state (*Dm*AK WT_{apo}; PDB ID: 6KY2) and its mutant with L-arginine (H284A-Arg; PDB ID: 6KY3) belonged to the C2 space group with unit cell parameters of a = 78.00 Å, b = 57.89 Å, c = 74.45 Å, β = 100.09°, and a = 77.94 Å, b = 57.84 Å, c = 74.86 Å, β = 100.46°. Each crystal was evaluated as a monomer per asymmetric unit with Matthews's coefficient parameters of V_M = 2.06 $Å^3D^{-1}$, 40.3%, and V_M = 2.07 $Å^3D^{-1}$, 40.5% of solvent content, respectively. Structural analysis of *Dm*AK WT_{apo} and H284A-Arg was conducted by molecular replacement at 1.87 Å and 1.34 Å resolution. The final models have R_{work} value of 18.73% and R_{free} of 23.01%, and R_{work} of 17.35% and R_{free} of 21.83%, respectively.

As mentioned above, the crystal structures of *Dm*AK WT_{apo} and H284A-Arg adopt a monomeric form in an asymmetric unit. Unfortunately, both crystal structures are missing two amino acids (E297-E298) in *Dm*AK WT_{apo} and nine amino acids (T311-E319) in H284A-Arg, well-known as the specific loop, including G310-V322 in the antiparallel β-sheet region. This absence might be due to very high structural flexibility. In addition, both monomeric structures consist of an N-terminal domain arranged with an irregular bundle of helical structures and a C-terminal domain containing eight-stranded antiparallel β-sheets, enclosed by four long α-helical structures. Their overall topologies showed no significant difference in the superimposed structure between *Dm*AK WT_{apo} and H284A-Arg using the Superpose program in CCP4 (root-mean-square deviation [r.m.s.d] = 0.22 Å for Cα atoms) (Fig. 3A) (Krissinel and Henrick, 2004). In contrast to the H284A-Arg structure, the specific loop, well defined by electron density map in the *Dm*AK WT_{apo} structure, was modeled completely (Fig. 3B). Analysis of the arginine binding site of

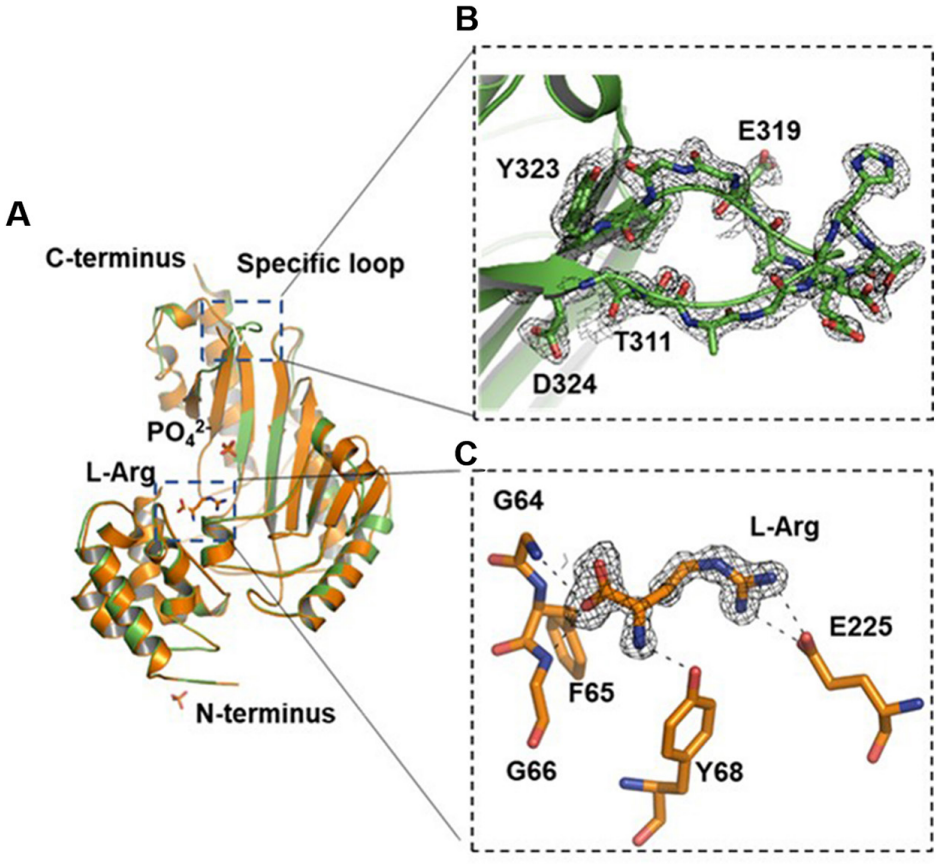

Fig. 3. Structure comparison between *Dm*AK WT_{apo} (PDB entry: 6KY2) and H284A-Arg (PDB entry: 6KY3). (A) Superimposed structures between *Dm*AK WT_{apo} (green) and H284A-Arg (orange) shown as cartoon model. (B) Specific loop region in *Dm*AK WT_{apo} is presented by green cartoon and ball and stick model containing electron density map (2Fo-Fc; 1σ). (C) The binding site of the L-arginine substrate in the H284A-Arg structure. The binding mode of L-arginine at the substrate binding site is shown as dot lines (dark). The L-arginine is shown as stick model including the electron density map (2Fo-Fc; 1σ).

H284A-Arg showed that the L-arginine substrate binds to the same active site as previously reported AK structures (Fig. 3C) (Yousef et al., 2002; Zhou et al., 1998). Even though the H284A-Arg structure contains L-arginine, the structural change still did not occur. This finding suggests that arginine binding is not sufficient to cause structural change.

B-factor analysis of *Dm*AK WT in the apo-state and its mutant with arginine

Even though the overall topologies of *Dm*AKs showed no

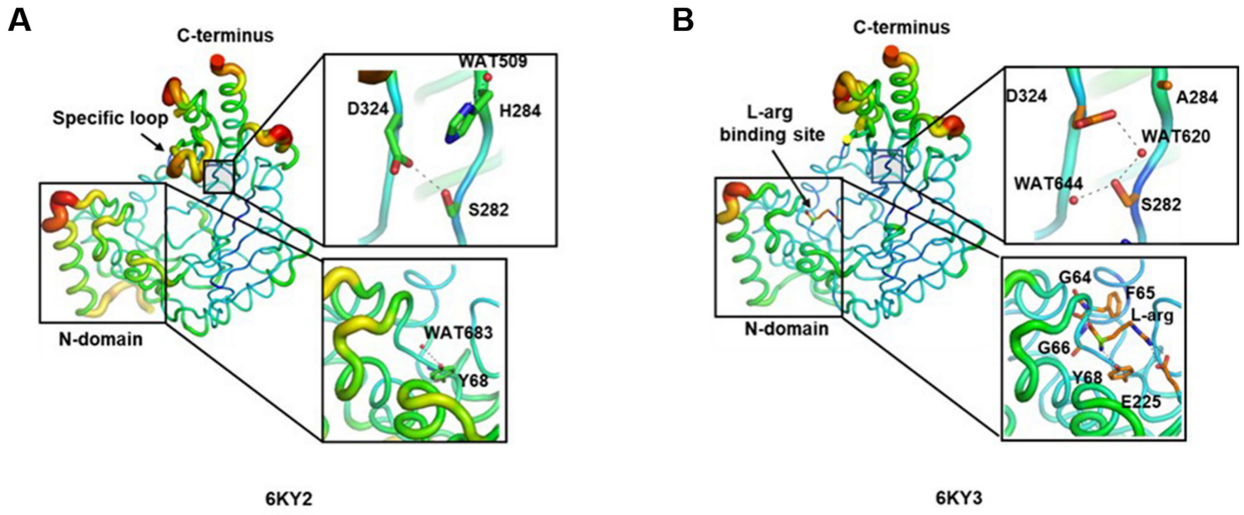

Fig. 4. Analysis of B-factor on *Dm*AK WT_{apo} (PDB ID: 6KY2) and H284A-Arg (PDB ID: 6KY3). The structures are presented in putty representation including rainbow color from red to violet in B-factor value order. Each box indicates regions with B-factor difference in the structural comparison of *Dm*AKs. (A) *Dm*AK WT_{apo}. (B) H284A-Arg.

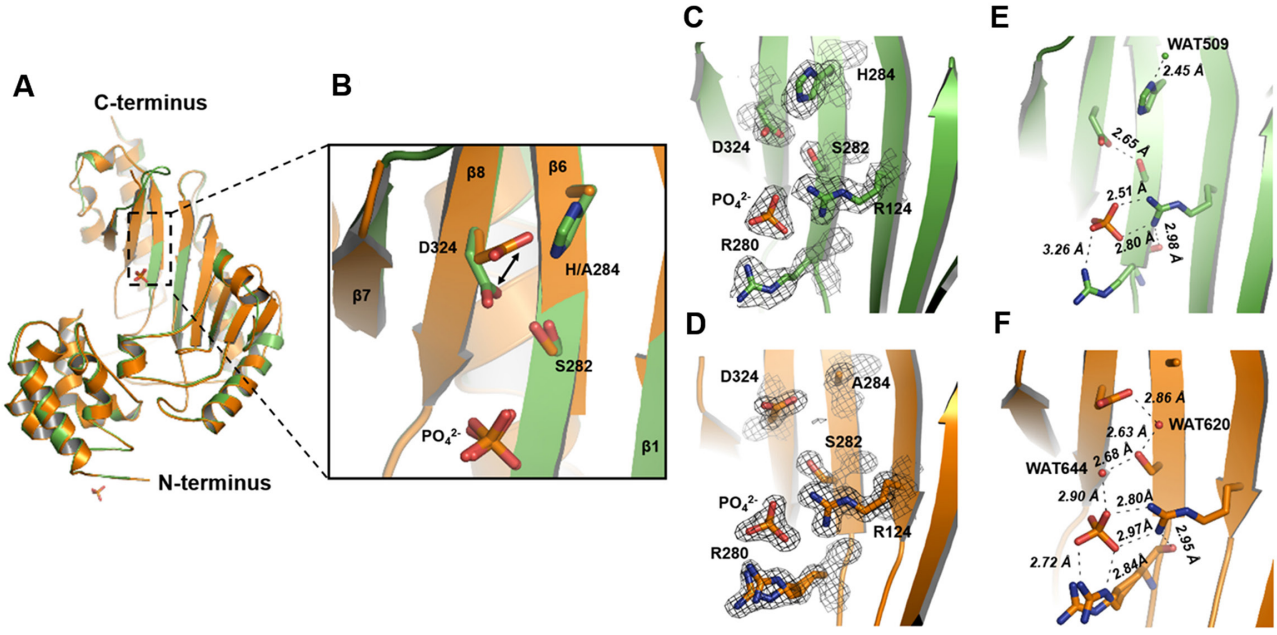

Fig. 5. Structural feature of *Dm*AK H284A-Arg structure (PDB ID: 6KY3) compared to WT_{apo} (PDB ID: 6KY2). (A) Superposition of *Dm*AK WT_{apo} and H284A-Arg. Each structure of *Dm*AK WT_{apo} and H284A-Arg is presented as a green and orange cartoon model, respectively. (B) Rotamer change of D324 in H284A-Arg structure. The black arrow indicates a structural change of D324. (C and D) The electron density map of amino acids and phosphate ion related to changes in the hydrogen bond network around the H284 residue (2Fo-Fc; 1σ). Their electron density maps were presented as black mash. (E and F) The hydrogen bond network in their c-domain. Water molecules are shown as a red sphere model. Dotted lines indicate hydrogen bonds, including distance.

significant structural differences, we investigated the structural flexibility to find clues of the detailed structural stability between both structures. The results revealed that there is a new water molecule in the L-arginine binding site of *Dm*AK WT_{apo} and differences of structural flexibility in the N-domain and around the H284 residue of *Dm*AK, respectively. Based on the B-factor comparison, we realized that the B-factor at the L-arginine binding site of *Dm*AK WT_{apo} is much higher than that of the H284A-Arg structure. The decreased structural flexibility of the N-domain in the H284A-Arg structure is induced by L-arginine binding, in contrast to the *Dm*AK WT_{apo} structure (Fig. 4A). Conversely, the structural flexibility around the A284 residue in the H284A-Arg structure, especially S282 residue, is lower than that of the wild type (Fig. 4B). This result was presumed due to the new hydrogen-bonded network produced through the destruction of π-stacking caused by H284A mutation.

Structural features of H284A-Arg structure

Compared with the *Dm*AK WT_{apo} structure, the crystal structure of H284A-Arg shows three unique features in the eight-stranded antiparallel β-sheets. These are a rotamer change of the D324 residue in the eighth beta-strand, a change in the hydrogen-bonding network, and disruption of π-stacking between the imidazole group of the H284 residue and the adenine ring of ADP. To examine structural changes in the H284A-Arg crystal structure, the *Dm*AK WT_{apo} structure was superimposed (Fig. 5A). In addition, as shown in Fig. 5B, the carboxyl group of the D324 residue in the H284A-Arg structure faces the A284 residue. The rotamer change of the D324 residue leads to an alteration of the hydrogen-bonding network around the ATP binding site (Figs. 5C-5F). The D324 residue in the H284A-Arg structure interacts with S282 mediated by a water molecule (WAT620), whereas the hydrogen bonds between D324 and S282 are formed directly in the *Dm*AK WT_{apo} structure. In particular, in contrast with the *Dm*AK WT_{apo} structure, the hydrogen bond network adjacent to the ATP binding site is mediated by WAT620 and WAT644 water molecules through alteration of D324, and this is extended to the R124 and R280 residues associated with ATP binding. In the previously reported AK structure with a TSA from *L. polyphemus* (*Lp*AK_{holo}; PDB ID: 1BG0), π-stacking between the imidazole group of the H284 residue and the adenine ring of ADP is shown in the nucleotide-binding site (Zhou et al., 1998). However, in the H284A-Arg structure, the π-stacking disappears upon mutation of H284. In the

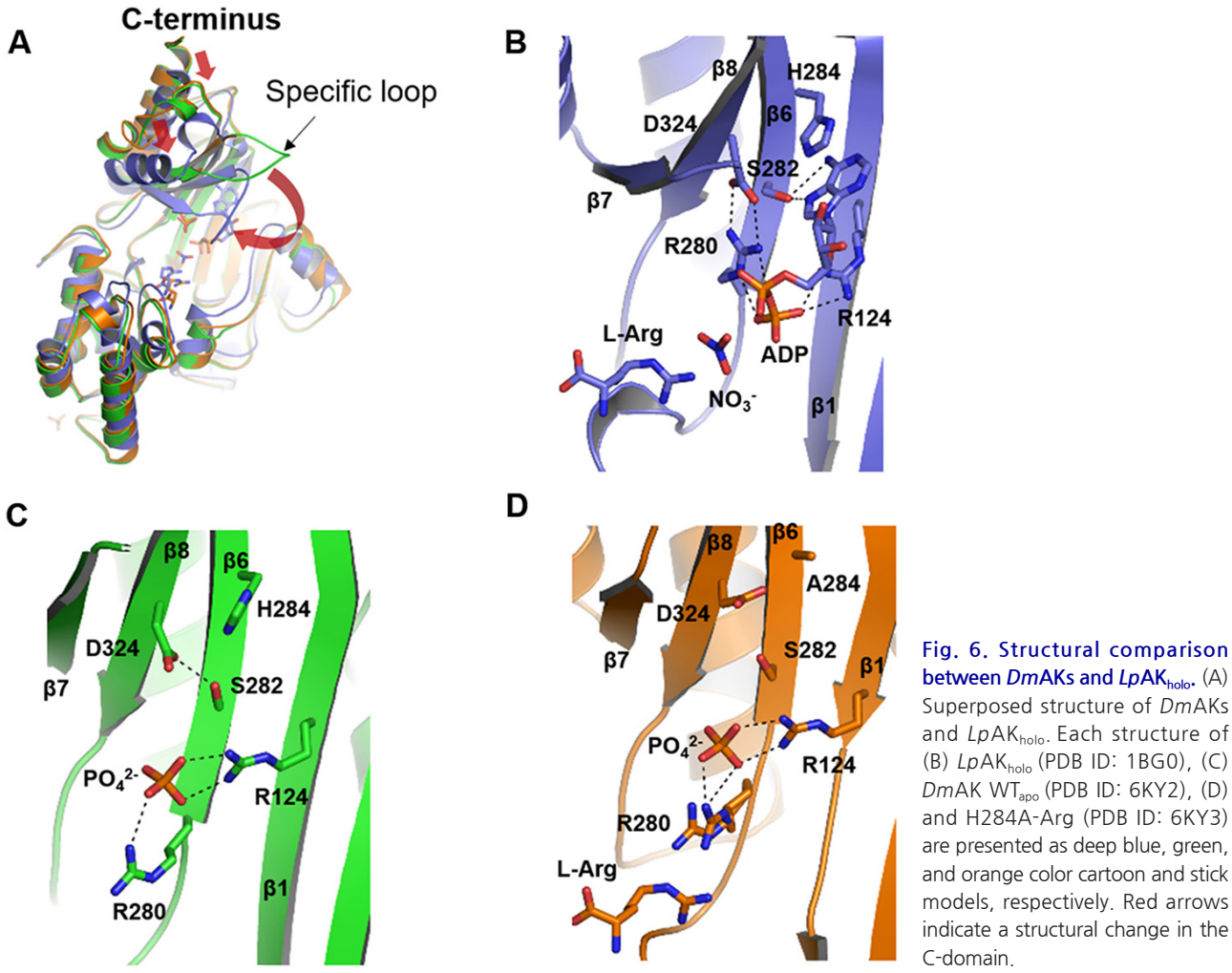

Fig. 6. Structural comparison between *Dm*AKs and *Lp*AK_{holo}. (A) Superposed structure of *Dm*AKs and *Lp*AK_{holo}. Each structure of (B) *Lp*AK_{holo} (PDB ID: 1BG0), (C) *Dm*AK WT_{apo} (PDB ID: 6KY2), (D) and H284A-Arg (PDB ID: 6KY3) are presented as deep blue, green, and orange color cartoon and stick models, respectively. Red arrows indicate a structural change in the C-domain.

overall structure of H284A-Arg, we posit that the disruption of π-stacking is related closely to the change of the D324 rotamer and the hydrogen-bonding network.

Structural comparison of *Dm*AK WT_{apo}, H284A-Arg, and *Lp*AK_{holo}

To examine the structural differences between the specific loops of the *Dm*AK WT_{apo}, H284A-Arg, and another AK structure with *Lp*AK_{holo}, *Lp*AK_{holo} was superimposed on *Dm*AKs (r.m.s.d = 2.73 Å for Cα atoms with *Dm*AK WT_{apo} and r.m.s.d = 2.42 Å for Cα atoms with H284A-Arg) (Fig. 6A) (Zhou et al., 1998). In terms of superposition between structures, the structure of *Dm*AK WT_{apo} is similar to that of H284A-Arg, apart from D324, which involves movements of helices and specific loop bending to the substrate-binding site (the adoption of a closed conformation), in the specific loop (G310-V322) connecting with β7 and β8. Furthermore, the *Lp*AK_{holo} structure shows the formation of a salt bridge between R280 and D324 (Fig. 6B). The salt bridge due to ADP binding might be related closely to the adoption of a closed conformation. In contrast to the *Lp*AK_{holo} structure, the salt bridge formation between R280 and D324 is not shown in the structures of *Dm*AK WT_{apo} and H284A-Arg. In the *Dm*AK WT_{apo} structure, the D324 is coordinated directly by S282 associated with ATP binding, whereas the D324 in the H284A-Arg structure interacts indirectly with S282 (Figs. 5F, 6C, and 6D) (Zhou et al., 1998). Interestingly, both structures contain a phosphate ion around the ATP binding site. The phosphate ion, which could be replaced with the β-position phosphate of ADP binding, is coordinated by R124 and R280 residues as in the previously reported crystal structure of *Lp*AK (Lopez-Zavala et al., 2013). However, the phosphate ion does not seem to play a sufficient role to account for the structural changes in the substrate-binding state. The reason is that the phosphate ion interferes with the formation of the salt bridge induced by ATP binding between R280 and D324, as shown in the *Lp*AK_{holo} crystal structure. Therefore, we assume that the reason for the difficult crystallization of *Dm*AK_{holo} for structural analysis under phosphate-containing conditions is due to the interference of the phosphate ion.

In conclusion, the rotamer change of D324 and the alteration of the hydrogen bond network could be induced by the disruption of π-stacking. The disruption of π-stacking in the H284A-Arg structure leads to a reduction in *Dm*AK activity. Thus, as shown in Table 1, the disruption of π-stacking has no significant effect on K_m and K_d values for either arginine or ATP, but only affects the V_{max} and k_{cat}. The structural changes induced by the disruption of π-stacking between the imidazole group of the H284 residue and the adenine ring of ADP may have an inhibitory effect on the induced fit model formation, which is a structural change caused by the binding of the substrates to *Dm*AKs.

Note: Supplementary information is available on the Molecules and Cells website (www.molcells.org).

ACKNOWLEDGMENTS

The authors appreciate the staff of Beamlines 7A at the Pohang Accelerator for their technical assistance during the data collection. This research was supported by the "Research Base Construction Fund Support Program" funded by Jeonbuk National University in 2019.

AUTHOR CONTRIBUTIONS

Z.R. and S.Y.K. designed and performed experiment, collected and analyzed data, and wrote manuscript. X.L. and D.S.K. performed the experiment, collected data. Y.J.K. and J.H.P. designed the experiments, edited the manuscript and managed the project.

CONFLICT OF INTEREST

The authors have no potential conflicts of interest to disclose.

ORCID

Zhili Rao https://orcid.org/0000-0002-8187-9023
So Young Kim https://orcid.org/0000-0002-5651-3046
Xiaotong Li https://orcid.org/0000-0002-9713-8836
Da Som Kim https://orcid.org/0000-0002-6146-4920
Yong Ju Kim https://orcid.org/0000-0003-2432-7190
Jung Hee Park https://orcid.org/0000-0002-4800-628X

REFERENCES

Adeyemi, O.S. and Whiteley, C.G. (2014). Interaction of metal nanoparticles with recombinant arginine kinase from *Trypanosoma brucei*: thermodynamic and spectrofluorimetric evaluation. Biochim. Biophys. Acta *1840*, 701-706.

Alonso, G.D., Pereira, C.A., Remedi, M.S., Paveto, M.C., Cochella, L., Ivaldi, M.S., Gerez de Burgos, N.M., Torres, H.N., and Flawia, M.M. (2001). Arginine kinase of the flagellate protozoa *Trypanosoma cruzi*. Regulation of its expression and catalytic activity. FEBS Lett. *498*, 22-25.

Azzi, A., Clark, S.A., Ellington, W.R., and Chapman, M.S. (2004). The role of phosphagen specificity loops in arginine kinase. Protein Sci. *13*, 575-585.

Baoyu, C., Qin, G., Zhi, G., and Xicheng, W. (2003). Improved activity assay method for arginine kinase based on a ternary heteropolyacid system. Tsinghua Sci. Technol. *8*, 422-427.

Bradford, M.M. (1976). A rapid and sensitive method for the quantitation of microgram quantities of protein utilizing the principle of protein-dye binding. Anal. Biochem. *72*, 248-254.

Brown, A.E. and Grossman, S.H. (2004). The mechanism and modes of inhibition of arginine kinase from the cockroach (*Periplaneta americana*). Arch. Insect Biochem. Physiol. *57*, 166-177.

Chen, L.H., Borders, C.L., Vasquez, J.R., and Kenyon, G.L. (1996). Rabbit muscle creatine kinase: consequences of the mutagenesis of conserved histidine residues. Biochemistry *35*, 7895-7902.

Clark, S.A., Davulcu, O., and Chapman, M.S. (2012). Crystal structures of arginine kinase in complex with ADP, nitrate, and various phosphagen analogs. Biochem. Biophys. Res. Commun. *427*, 212-217.

Ellington, W.R. (1989). Phosphocreatine represents a thermodynamic and functional improvement over other muscle phosphagens. J. Exp. Biol. *143*, 177-194.

Ellington, W.R. (2001). Evolution and physiological roles of phosphagen systems. Annu. Rev. Physiol. *63*, 289-325.

Emsley, P. and Cowtan, K. (2004). Coot: model-building tools for molecular graphics. Acta Crystallogr. D Biol. Crystallogr. *60*, 2126-2132.

Fernandez, P., Haouz, A., Pereira, C.A., Aguilar, C., and Alzari, P.M. (2007). The crystal structure of *Trypanosoma cruzi* arginine kinase. Proteins *69*, 209-212.

Forstner, M., Muller, A., Stolz, M., and Wallimann, T. (1997). The active site

histidines of creatine kinase. A critical role of His 61 situated on a flexible loop. Protein Sci. *6*, 331-339.

Gattis, J.L., Ruben, E., Fenley, M.O., Ellington, W.R., and Chapman, M.S. (2004). The active site cysteine of arginine kinase: structural and functional analysis of partially active mutants. Biochemistry *43*, 8680-8689.

Guo, Q., Chen, B., and Wang, X. (2004). Evidence for proximal cysteine and lysine residues at or near the active site of arginine kinase of *Stichopus japonicus*. Biochemistry (Mosc). *69*, 1336-1343.

Hansen, D.E. and Knowles, J.R. (1981). The stereochemical course of the reaction catalyzed by creatine kinase. J. Biol. Chem. *256*, 5967-5969.

Kabsch, W. (2010). Xds. Acta Crystallogr. D Biol. Crystallogr. *66*, 125-132.

Krissinel, E. and Henrick, K. (2004). Secondary-structure matching (SSM), a new tool for fast protein structure alignment in three dimensions. Acta Crystallogr. D Biol. Crystallogr. *60*, 2256-2268.

Li, M., Wang, X.Y., and Bai, J.G. (2006). Purification and characterization of arginine kinase from *locust*. Protein Pept. Lett. *13*, 405-410.

Liu, N., Wang, J.S., Wang, W.D., and Pan, J.C. (2011). The role of Cys271 in conformational changes of arginine kinase. Int. J. Biol. Macromol. *49*, 98-102.

Lopez-Zavala, A.A., Garcia-Orozco, K.D., Carrasco-Miranda, J.S., Sugich-Miranda, R., Velazquez-Contreras, E.F., Criscitiello, M.F., Brieba, L.G., Rudino-Pinera, E., and Sotelo-Mundo, R.R. (2013). Crystal structure of shrimp arginine kinase in binary complex with arginine-a molecular view of the phosphagen precursor binding to the enzyme. J. Bioenerg. Biomembr. *45*, 511-518.

McCoy, A.J., Grosse-Kunstleve, R.W., Adams, P.D., Winn, M.D., Storoni, L.C., and Read, R.J. (2007). Phaser crystallographic software. J. Appl. Crystallogr. *40*, 658-674.

Muhlebach, S.M., Gross, M., Wirz, T., Wallimann, T., Perriard, J.C., and Wyss, M. (1994). Sequence homology and structure predictions of the creatine-kinase isoenzymes. Mol. Cell. Biochem. *133*, 245-262.

Murshudov, G.N., Vagin, A.A., and Dodson, E.J. (1997). Refinement of macromolecular structures by the maximum-likelihood method. Acta Crystallogr. D Biol. Crystallogr. *53*, 240-255.

Newsholme, E.A., Beis, I., Leech, A.R., and Zammit, V.A. (1978). The role of creatine kinase and arginine kinase in muscle. Biochem. J. *172*, 533-537.

Niu, X., Bruschweiler-Li, L., Davulcu, O., Skalicky, J.J., Bruschweiler, R., and Chapman, M.S. (2011). Arginine kinase: joint crystallographic and NMR RDC analyses link substrate-associated motions to intrinsic flexibility. J. Mol. Biol. *405*, 479-496.

Noh, E.J., Kang, S.W., Shin, Y.J., Kim, D.C., Park, I.S., Kim, M.Y., Chun, B.G., and Min, B.H. (2002). Characterization of mycoplasma arginine deiminase expressed in *E. coli* and its inhibitory regulation of nitric oxide synthesis. Mol. Cells *13*, 137-143.

Pereira, C.A., Alonso, G.D., Paveto, M.C., Iribarren, A., Cabanas, M.L., Torres, H.N., and Flawia, M.M. (2000). *Trypanosoma cruzi* arginine kinase characterization and cloning. A novel energetic pathway in protozoan parasites. J. Biol. Chem. *275*, 1495-1501.

Pruett, P.S., Azzi, A., Clark, S.A., Yousef, M.S., Gattis, J.L., Somasundaram, T., Ellington, W.R., and Chapman, M.S. (2003). The putative catalytic bases have, at most, an accessory role in the mechanism of arginine kinase. J. Biol. Chem. *278*, 26952-26957.

Rao, Z., Kim, S.Y., Akanda, M.R., Lee, S.J., Jung, I.D., Park, B.Y., Kamala-Kannan, S., Hur, J., and Park, J.H. (2019). Enhanced expression and functional characterization of the recombinant putative lysozyme-PMAP36 fusion protein. Mol. Cells *42*, 262-269.

Schrödinger (2010). The PyMOL Molecular Graphics System, version 1.3r1 (New York: Schrödinger).

Strong, S.J. and Ellington, W.R. (1996). Expression of horseshoe crab arginine kinase in *Escherichia coli* and site-directed mutations of the reactive cysteine peptide. Comp. Biochem. Physiol. B Biochem. Mol. Biol. *113*, 809-816.

Suzuki, T., Fukuta, H., Nagato, H., and Umekawa, M. (2000a). Arginine kinase from *Nautilus pompilius*, a living fossil. Site-directed mutagenesis studies on the role of amino acid residues in the Guanidino specificity region. J. Biol. Chem. *275*, 23884-23890.

Suzuki, T., Yamamoto, Y., and Umekawa, M. (2000b). *Stichopus japonicus* arginine kinase: gene structure and unique substrate recognition system. Biochem. J. *351*, 579-585.

Takeuchi, M., Mizuta, C., Uda, K., Fujimoto, N., Okamoto, M., and Suzuki, T. (2004). Unique evolution of Bivalvia arginine kinases. Cell. Mol. Life Sci. *61*, 110-117.

Uda, K., Tanaka, K., Bailly, X., Zal, F., and Suzuki, T. (2005). Phosphagen kinase of the giant tubeworm *Riftia pachyptila*. Cloning and expression of cytoplasmic and mitochondrial isoforms of taurocyamine kinase. Int. J. Biol. Macromol. *37*, 54-60.

Watts, D.C., Anosike, E.O., Moreland, B., Pollitt, R.J., and Lee, C.R. (1980). The use of arginine analogues for investigating the functional organization of the arginine-binding site in lobster muscle arginine kinase. Role of the 'essential' thiol group. Biochem. J. *185*, 593-599.

Wu, Q.Y., Guo, H.Y., Geng, H.L., Ru, B.M., Cao, J., Chen, C., Zeng, L.Y., Wang, X.Y., Li, F., and Xu, K.L. (2014). T273 plays an important role in the activity and structural stability of arginine kinase. Int. J. Biol. Macromol. *63*, 21-28.

Wu, Q.Y., Li, F., and Wang, X.Y. (2008). Evidence that the amino acid residue P272 of arginine kinase is involved in its activity, structure and stability. Int. J. Biol. Macromol. *43*, 367-372.

Wyss, M. and Kaddurah-Daouk, R. (2000). Creatine and creatinine metabolism. Physiol. Rev. *80*, 1107-1213.

Yousef, M.S., Fabiola, F., Gattis, J.L., Somasundaram, T., and Chapman, M.S. (2002). Refinement of the arginine kinase transition-state analogue complex at 1.2 Å resolution: mechanistic insights. Acta Crystallogr. D Biol. Crystallogr. *58*, 2009-2017.

Zhou, G., Somasundaram, T., Blanc, E., Parthasarathy, G., Ellington, W.R., and Chapman, M.S. (1998). Transition state structure of arginine kinase: implications for catalysis of bimolecular reactions. Proc. Natl. Acad. Sci. U. S. A. *95*, 8449-8454.